Realization of porous silicon photonic bandgap optical sensor devices

P. N. PATEL, VIVEKANAND MISHRA*, (SMIEEE)
Electronics Engineering Department, S. V. National Institute of Technology, Surat-395007, Gujarat, India

Recently, Porous Silicon (PS) is emerged as a new, unique and promising material for the optoelectronic devices and the sensing applications. This paper reports the feasibility for realization of one dimensional (1D) PS Photonic Bandgap (PBG) sensor devices. Different 1D-PSPBG sensor device structures such as single layer, Distributed Bragg Reflector (DBR) and microcavity were fabricated by electrochemical anodization of crystalline silicon wafer and proposed as a large surface area matrix for optical sensing applications. The refractive index of the 1D-PSPBG structure is tuned by changing current density and the thickness by etching time. Wavelength shift (Δλ) in the measured reflectance spectra of prepared structures were analyzed for the detection of the analyte in the porous structure. The sensing device performance is tested by the different organic chemicals and it showed good linear relation between the refractive index of analyte inside the pores and the wavelength shift.

(Received February 13, 2012; accepted March 13, 2014)

Keywords: Porous silicon, Photonic bandgap structures, Optical sensor, Electrochemical anodization

1. Introduction

Selective and accurate sensing of different analytes such as chemical, biochemical and biological analyte is today's prime need. Optical sensor field is motivated by the expectation that it has significant advantages [1] compared to conventional electronic-based sensors. PBG structures are periodic dielectric structures that control the propagation of electromagnetic wave through the photonic crystal [2]. Due to the ability to sense very small refractive index change of a medium, PBG structures have attracted the scientists and researchers [3]. In recent years, PS is emerged as a promising nano PBG structure due to tremendous advantages in nano scale optical devices and sensing applications [4-5]. Many groups all over the world have been working in the research to develop nano sensors using PS for the current and the future applications, because its optical properties are highly sensitive to the presence of chemical and biological species inside the pores [6]. Several groups have reported the applications of PS nano structures in the optical devices and sensing applications. Fauchet et al. reported work on the optical biosensors applications using nano structure PS [7]. They report significant wavelength shift in the reflectance spectra for the different bio-analytes. C. S. Solanki et al. demonstrated the photovoltaic solar cell applications using PS [8]. They reported increased efficiency of the solar cell using PS material. Sailor research group works on the drug delivery devices and materials using PS [9]. They review and demonstrate the preparation, chemistry and properties of electrochemically prepared PS hosts relevant to drug delivery applications. Apart from these, many research groups are doing research related to characterization and other emerging and future nano technology applications using PS [10-14].

The objective of this work is to evaluate the feasibility for realization of 1D-PSPBG sensing matrix device structures such as single layer, DBR and microcavity by electrochemical anodization. First, experimental detail for the fabrication of 1D-PSPBG sensing device structures is presented. Then, the principle of interferometric optical sensing, structural and optical characterization of sensing device structure is discussed. Finally, the testing of these sensing device structures have been studied for the sensing of organic solvents such as methanol, ethanol, propanol and benzene by examining the wavelength shift in their reflectance spectra before, during and after exposure.

2. Experimental

1D-PSPBG single layer and multilayer structures, such as DBR and microcavities were fabricated by electrochemical etching of p-type Si wafer (<100>, 0.01-0.02 ohm-cm, 275 μm, 20 cm^2). The schematic diagram of the electrochemical etching cell is shown in Fig. 1.

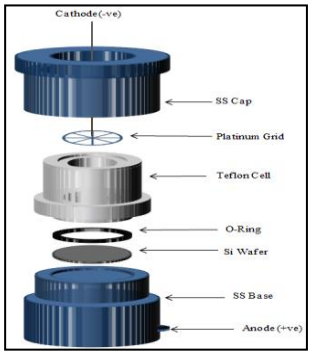

Fig. 1. Electrochemical etching cell.

As shown in Fig. 1, the base and the cap of the electrochemical etching cell were made with SS 320 metal. Silicon wafer was placed inside the base and sealed with an O-ring and exposed to the electrolyte. The electrolyte mixture was kept in the highly HF resistant polymer polytetrafluoroethylene (PTFE), which was in contact with the platinum grid, used as a cathode. First, silicon wafer was cleaned using standard piranha cleaning method. PTFE bath was filled with the etching solution of 40% aqueous HF and 99% ethanol, mixed in the ratio of 1:2. The cathode was immersed in the electrolyte solution and the distance between anode and cathode was kept about 4.5 cm. Periodic constant current square wave was applied by programmable DC power supply (PWS 4305, Tektronix). A constant current mode was used for anodization process as it is beneficial in terms of regulation [15]. Applied current density (J) and the etching time (t) profile are responsible for the change in refractive index (n) and the physical thickness (d) profile of the layer, respectively. The fabrication schematic diagram of the single layer, DBR and microcavity structure is shown in Fig. 2 (a), (b) and (c) respectively. In Fig. 2, n_s is the refractive index of the substrate and N is the number of period. First, single layer structure was fabricated by applying current density 70 mA/cm^2 for the 60 sec. for one repetition (Fig. 2 (a)). Multilayer DBR was fabricated with twenty repetitions of current density and etching time sequences as shown in Fig. 2 (b). The microcavity was realized by inserting a cavity layer of high current density between two identical DBR1 and DBR2 with six repetitions of a current density and etching time sequences as shown in Fig. 2 (c).

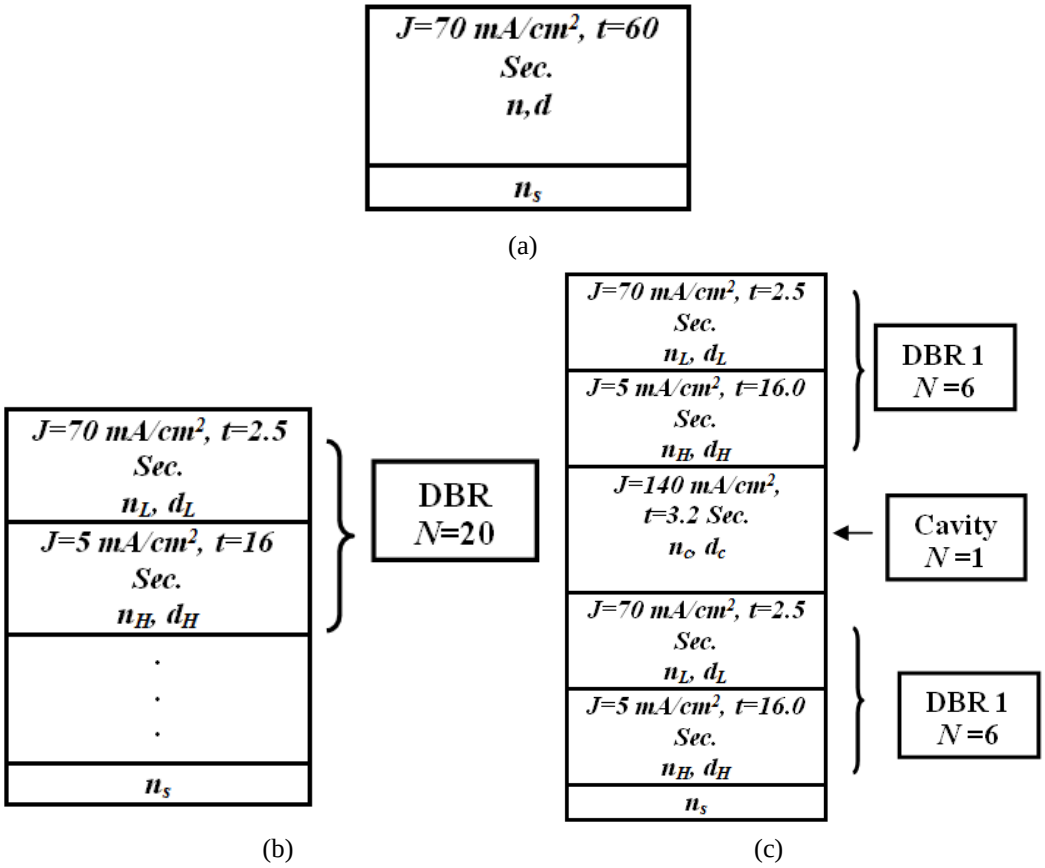

Fig. 2. Fabrication Schematic of (a) Single layer (b) DBR and (c) Microcavity Structure.

After electrochemical etching, these structures were rinsed in DI water for 10 minutes and dried at room temperature. Structural morphology (plan and cross sectional view) was examined by SEM (CHI900B CH Instruments). The reflectance spectra were measured before, during and after exposure to various organic solvents using spectrometer (MayaPro-2000, Ocean Optics). All measurements were done in the air. Polished silicon wafer was used as reference in the reflectance measurements.

3. Results and discussion

According to the optics theory, the reflectance spectrum of 1D-PSPBG structure is governed by the interferometric Fabry-Perot relationship [16-17]. Light reflected from the top interface (air-PS) and the bottom interface (PS-Si substrate) interfere with each other and form the typical Fabry-Perot fringes in the reflectance spectrum. The fringe pattern is closely related to effective optical thickness, which is product of physical thickness

and refractive index of the structure, by the relationship shown in as:

$$m\lambda = 2nd \quad (1)$$

where, m is an integer (the spectral peak order) and λ is the peak wavelength. For bare 1D-PSPBG structure (without any analyte), the refractive index of the structure is n. When the pores are filled with an analyte (e.g., chemicals or bio-chemicals), the effective refractive index of the structure increases from n to $n+\Delta n$ with shift in wavelength from λ to $\lambda+\Delta\lambda$ in the reflectance spectra due to increased optical thickness of the structure. For the multilayer 1D-PSPBG structures with alternating high refractive index layers and low refractive index layers the Eq. (1) becomes:

$$\frac{m\,\lambda_0}{2} = n_L d_L + n_H d_H \quad (2)$$

where, λ_0 is the photonic resonance wavelength, n_L and d_L are the refractive index and the thickness of the low index layer, respectively, while n_H and d_H *are* the refractive index and the thickness of the high index layer, respectively.

The prepared structures show distinct green, blue and red colours distribution over the entire surface (Fig. 3). Porous structure in the bulk silicon is strongly responsible for the change in the surface colour due to the shifting in the bandgap energy of silicon [18].

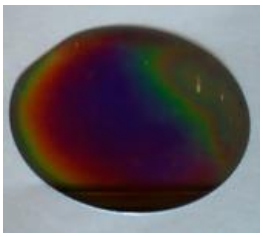

a) DBR

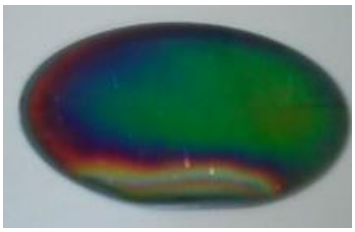

b) Microcavity

Fig. 3. Fabricated 1D-PSPBG structures.

First layer of each structure is fabricated using the current density (J=70 mA/cm^2), hence the plan view of each structure is same. Fig. 4 shows the surface morphology of the structures in SEM plan view. The array of void spaces (dark) in silicon matrix (bright) can be seen clearly in the plan view SEM image. The morphology of the structures shows that the electrochemical etching is done uniformly on the surface and created the granular structure in a spherical shape. Large number of pores distributed in all direction can be observed in Fig. 4 with mean pore size of 24 nm measured using Image J software [19].

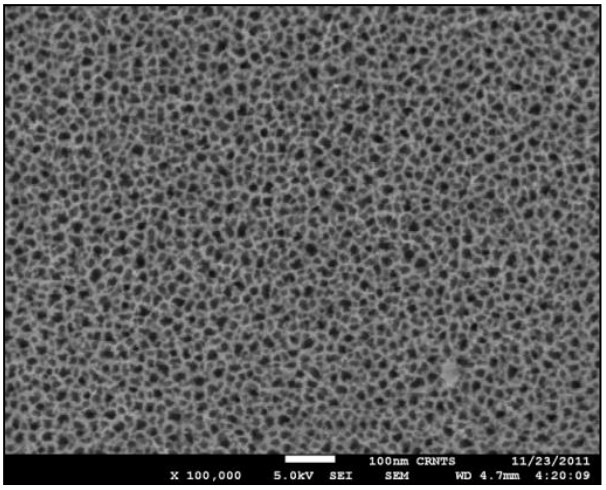

Fig. 4. SEM Plan View of 1D-PSPBG structures.

The cross-sectional images of the DBR and microcavity multilayer structures are shown in Fig. 5 (a) and (b), respectively. Multilayered stacks are clearly observed in these figures. These stacks are due to the periodic variation in the refractive index profile through the current density variation for different etching time. The cavity layer of the microcavity structure can be clearly observed in the inset figure of Fig. 5 (b). The thickness of the cavity layer is 229.88 nm, measured using Image J software.

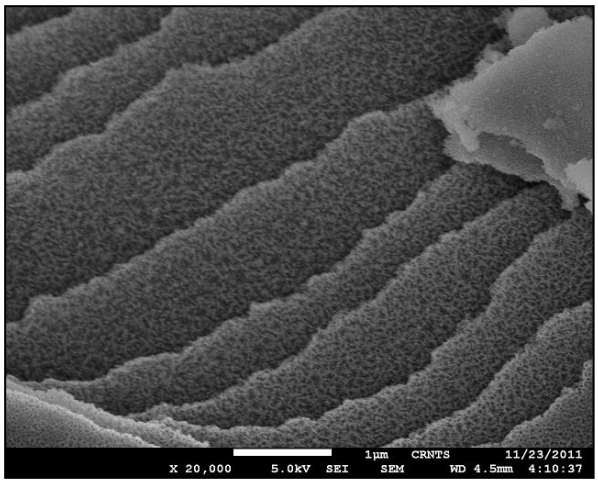

Fig. 5 (a). SEM Cross-section Images of DBR .

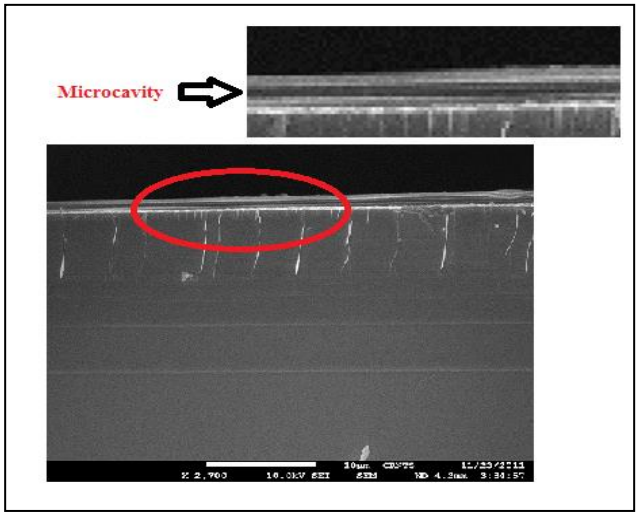

Fig. 5 (b). SEM Cross-section Images of Microcavity.

As seen in Fig. 5 (c), the light grey stripes correspond to low porosity layers for the current density 5 mA/cm^2 (high refractive index) and the dark gray stripes correspond to high porosity layers for the current density 70 mA/cm^2 (low refractive index) . The thickness of the high refractive index layer (J=5 mA/cm^2) is 72 nm and low refractive index layer (J=70 mA/cm^2) is 110 nm measured using Image J software. Further, the branched cylindrical structure possessed by the pores, is also clearly visible in Fig. 5 (c); which shows that the pore growth is occurred in the depth (perpendicular to the surface) of the structure.

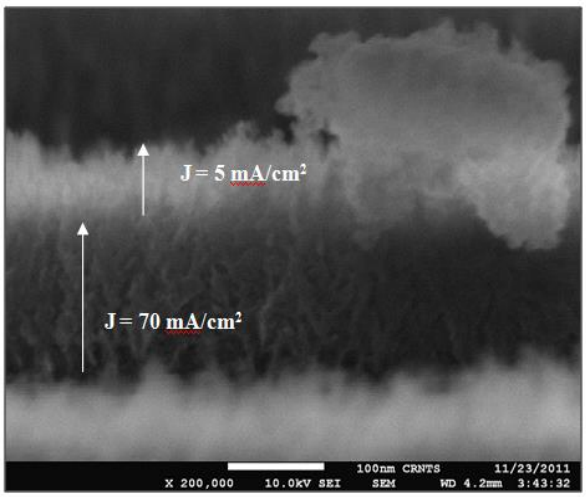

Fig. 5 (c). Low and High Porosity layers.

After drying of single layer, DBR and microcavity structures at room temperature, the reflectance spectra were measured for these structures, which are shown in Fig. 6 (a), (b) and (c), respectively.

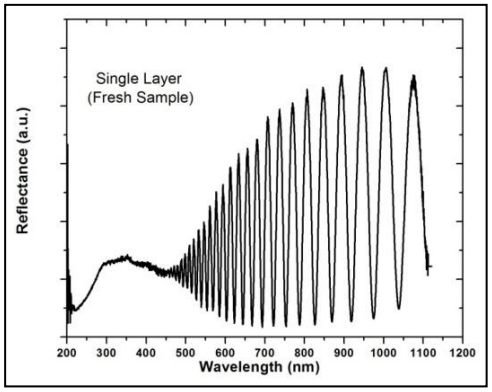

(a)

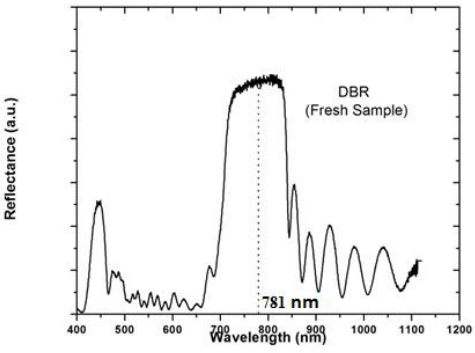

(b)

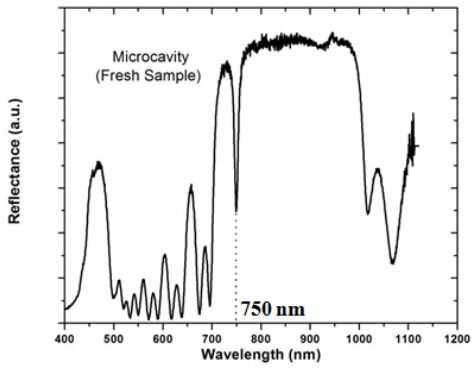

(c)

Fig. 6. Reflectance spectra of (a) single layer (b) DBR and (c) microcavity structures.

As shown in Fig. 6 (a), fringes in the reflectance spectrum was observed for the single layer structure, because it is a two phase composite mixture of air and the silicon solid phase. The photonic resonance centered at 781 nm and 750 nm is observed in the reflectance spectrum of DBR and microcavity structures respectively. The presence of small peaks between 400 to 500 nm for DBR and microcavity structures was observed in the reflectance spectra of Fig. 6 (b) and (c) respectively. This is due to the refractive index dispersion at those high energies. The reason behind this might be the absorption of light by PS at that wavelength since the refractive index is not constant at that energy range [20].

After realization and characterization of 1D-PSPBG sensor device structures, their performance as the sensor device was tested by analysing the wavelength shift in the

reflectance spectra during their exposure to 100% concentration of methanol, ethanol, propanol and benzene. Variations in the reflectance spectra of these sensing device structures during exposure to organic solvents are shown in the Fig. 7 (a), (b) and (c) respectively. During the adsorption, wavelength in the reflectance spectra promptly shifted toward the higher wavelength or low energy regions. This phenomenon can be attributed to the capillary adsorption of these organic solvents within the pores of the structures. The reference/resonant wavelength of the single layer, DBR and microcavity bare structure without any analyte structure, is taken as 807 nm, 781 nm and 750 nm, respectively. The wavelength shift measured from the reflectance spectra of 1D-PSPBG structures for the different organic solvents is listed in Table 1.

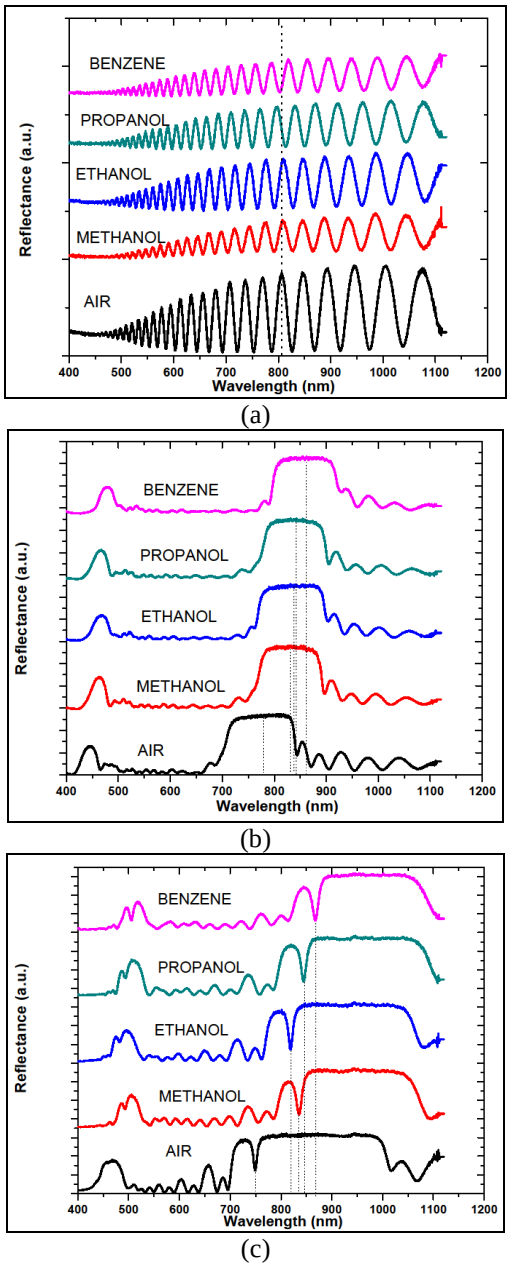

Fig. 7. Wavelength Shift (Δλ) in the Reflectance Spectra of (a) Single layer (b) DBR and (c) Microcavity Structure before and after Organic Solvents Adsorption.

It is clearly observed that the wavelength in the reflectance spectra of the 1D-PSPBG structure were shifted to higher wavelength, because the pores were filled with organic solvent (n > 1.0). The filled pores with organic solvent increase the overall effective refractive index of the structure and consequently increasing their optical thickness. This effect promotes the wavelength shift in the reflectance spectrum. The strength of the wavelength shift depends on the type of the 1D-PSPBG structure and the type of the organic solvent; because the effective refractive index of each 1D-PSPBG structure as well as organic solvent is different. Higher the refractive index of the structure and the solvent, higher the wavelength shift is observed.

Table 1. Wavelength Shift in Reflectance Spectra of 1D-PSPBG Structures after Organic Solvents Adsorption.

Organic Solvent	Refractive Index of Solvent (n) [23]	Δλ (nm)		
		Single Layer	DBR	Microcavity
Methanol	1.328	2.50	50.00	84.00
Ethanol	1.361	4.00	57.00	71.50
Propanol	1.385	8.00	61.00	95.00
Benzene	1.501	13.00	79.00	130.00

As shown in the Table 1, the standard variations in the wavelength of the multilayer PS structure are consistently higher than those of the single layer structure. This is due to the different structural properties of these structures. Due to multilayer structure of the DBR and microcavity, its effective refractive index is higher than the single layer structure (as per Eq. (2)) and hence the optical thickness are much larger than that of single layer structure during exposure to the solvents.

The relationship between refractive index of the organic solvent and the wavelength shift is plotted in Fig. 8 from the results of Table 1. Fig. 8 shows the good linear fitting for the graph of the refractive index values *vs.* wavelength shift. As shown in the Fig. 8, when the structure was exposed to organic solvents of a high refractive index, large variations in the reflectance spectra were observed; correspondingly, when the structure was exposed to organic solvents of a low refractive index, small variations in the reflectance spectra were observed in each case. This is due to the variations in the effective refractive index of the 1D-PSPBG layers according to the type of organic solvent adsorbed in its pores. In the Fig. 8, it is observed that almost all the experimental points are on the linear fitting curve except few points. The origin of the mismatch of few points may be due to some type of chemical reaction of this solvent with the surface of the structure.

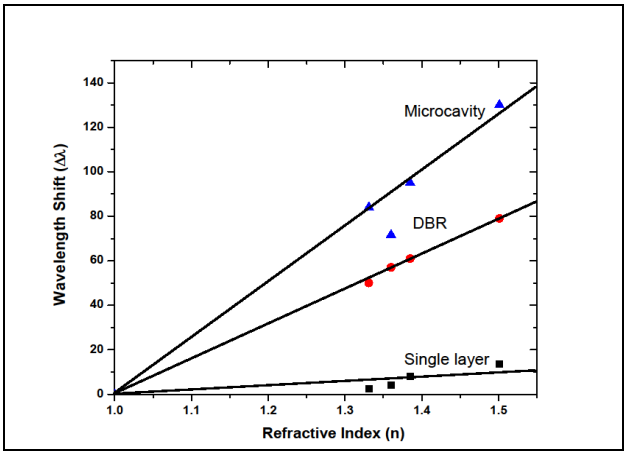

Fig. 8. Refractive Index vs. Wavelength Shift.

Sensitivity is one of the most important issues to evaluate the performance of the sensors. In this case, the response of the sensor structure was evaluated throughout the change of the wavelength shift in the reflectance spectrum for different solvents. This parameter showed to be a good indicator for sensing measurement in the 1D-PSPBG sensing devices. It is observed from Table 1 and Fig. 8 that, the performance of single layer structure is poor due to lack of reference as well as low wavelength shift due to structural properties. DBR structure gives better wavelength shift compared to single layer but still measurement accuracy is moderate. Compared to both of these structures, wavelength shift in the microcavity structure was consistently higher than other structures, because of its structural properties. Also, high measurement accuracy is obtained because it is much easier to resolve small shift in the reflectance spectrum of microcavity due to sharp resonance peak in the reflectance spectra.

It is also observed that, after complete evaporation of each organic solvents, the reflectance spectra of the structures promptly returns to their original waveform position. This implies that the change in reflectance spectra is indicative of the presence or absence of organic solvents in the pores and that the change in the spectra of the 1D-PSPBG structure is temporary. These results are very much useful for the development of effective reversible 1D-PSPBG based organic solvent sensors.

4. Conclusions

PS based single layer, DBR and microcavity photonic bandgap sensing device structures were fabricated by electrochemical etching. Porous structure is confirmed in the plan view of SEM characterization. Large number of pores uniformly distributed on overall surface with average 24 nm sizes is observed. Multilayered structure with periodic variation of the refractive indices is observed in the cross sectional SEM characterization. The thickness of the high refractive index layer is 72 nm, low refractive index layer is 110 nm and for the cavity layer is 229.88 nm which are measured using Image J software. The branched cylindrical structure possessed by the pores is observed in the cross sectional SEM image, which confirmed the pore growth in the depth of the structure. Optical characterization shows resonance wavelength of 781 nm and 750 nm for the DBR and the microcavity structures, respectively.

Testing of sensing device structures is done by the optical sensing of organic solvents like methanol, ethanol, propanol and benzene. It is observed that due to capillary adsorption of the organic solvents in the pores of the porous structures, the effective optical thickness and the refractive index of the structure changes which results in the wavelength shift in the reflectance spectra. Good linear fitting for the different 1D-PSPBG structure as a sensor device is observed. The microcavity structure showed to have a higher sensitivity for the different solvents. It is also, observed that, after complete evaporation of the organic solvents from the pores, the reflectance spectra of the structures promptly returns to their original waveform position. This is a very good quality of these structures, as it is helpful in the development of a reversible sensing device.

Acknowledgment

This work was supported by the grant from Defence Research and Development Organization (DRDO), Govt. of India. Authors are also thankful to CRNTS, SAIF, IIT Bombay for the structural characterization of the samples.

References

[1] Giancarlo C. Righini, Antonella Tajani, Antonello Cutolo (eds.), "An Introduction to Optoelectronic Sensors", World Scientific Publishing Co. Pvt. Ltd., (2009).
[2] J. E. Lugo, H. A. Lopez, S. Chan, P. M. Fauchet, J. Appl. Phys., **91**, 4966 (2002).
[3] A. Banerjee, Progress In Electromagnetics Research, **89**, 11 (2009).
[4] Shuan Ming Li, Fu Ru Zhong, Zhen Hong Jia, Min Tian, Advanced Materials Research, **236**, 1811 (2011).
[5] N. Koshida (ed.), "Device Applications of Silicon Nanocrystals and Nanostructures", Springer Science, 1st Ed., (2009).
[6] A. G. Cullis, L. T. Canham, P. D. J. Calcott, J. Appl. Physics, **82**, 3 (1997).
[7] Huimin Ouyang, Philippe M. Fauchet, SPIE Optics East, **6005**, 600508 (2005).
[8] A. K. Panchal, P. G. Kale, C. S. Solanki, ICAER, 797, (2007).
[9] Emily J. Anglin, Lingyun Cheng, William R. Freeman, Michael J. Sailor, Advanced Drug Delivery Reviews, **60**, 11 1266 (2008).
[10] R. S. Dubey, D. K. Gautam, Chalcogenide Letters **6**, 10 (2009).
[11] M. A. Mahdi, Asmiet Ramizy, Z. Hassan, S. S. Ng, J. J. Hassan, S. J. Kasim, Chalcogenide Letters **9**, 1 (2012).

[12] R. S. Dubey, D. K. Gautam, Journal of Optoelectronic and Biomedical Materials 1, 1 (2009).
[13] A. Mortezaali, S. Ramezani Sani, F. Javani Jooni, Journal of Non-Oxide Glasses, 1, 3 (2009).
[14] A. Ioanid, M. Dieaconu, S. Antohe, Digest Journal of Nanomaterials and Biostructures, 54, (2010).
[15] P. G. Kale, A. K. Panchal, C. S. Solanki, National Conf. on the Emerging Trends in the Photovoltaic Energy Generation & Utilization (NCETPEGU), 77, (2007).
[16] Hee-Kyung Min, Ho-Sik Yang, Sung M. Cho., Sensors and Actuators B, **67**,199, (2000).
[17] Han-Jung Kim, Young-You Kim, Ki-Won Lee, Horchhong Cheng and Dong Han Ha, Physica B, **406**, 1536, (2011).
[18] R. Dubey, D. K. Gautam, Opt. Quant. Electron, **41**, 189 (2009).
[19] W. S. Rasband, "Image J", National Institute of Health, Bethesda, Maryland, USA, http://rsb.info.nih.gov.ij/.
[20] A. Bardaoui, R. Bchir, H. Hamzaoui, R. Chtourou, Eur. Phys. J. Appl. Phys., **51**, 30701 (2010).
[21] Tables of Physical & Chemical Constants. 2.1.2 Barometry. Kaye & Laby Online. Version 1.1 (2008), http://www.kayelaby.npl.co.uk/chemistry/3_3/3_3.html.

*Corresponding author: vive@eced.svnit.ac.in